APPLICATION OF ARTIFICIAL NEURAL NETWORK (ANN) FOR PREDICTION OF DRAG COEFFICIENT OF AXISYMMETRIC BOATTAIL MODELS

Quang Nguyen Dinh[1], The Hung Tran[1], Gopal Sharma[2], and Jun Tanimoto[2,3]

[1]Faculty of Aerospace Engineering, Le Quy Don Technical University, Hanoi, Vietnam
[2]Interdisciplinary Graduate School of Engineering Sciences, Kyushu University, Fukuoka, 816-8580, Japan
[3]Faculty of Engineering Sciences, Kyushu University, Fukuoka, 816-8580, Japan

Abstract

The utilization of longitudinal grooves has demonstrated effectiveness in reducing drag on axisymmetric boattail models. However, the intricate relationship between groove parameters and drag force defies simple physical equations, necessitating the discovery of an optimal parameter set. Conventional experimental and numerical simulation approaches prove impractical due to their resource-intensive nature. Instead, Artificial Neural Networks (ANNs) offer a promising alternative. In this study, a three-layer ANN is trained using 192 examples generated by Ansys Fluent with the Reynolds-Averaged Navier-Stokes (RANS) method and the *k-ω* SST model. Subsequently, 48 examples are employed for network validation. Comparison between ANN-predicted values and CFD-determined drag coefficients reveals an average difference of less than 0.76%, validating the network's reliability. The ANN successfully identifies optimal groove parameters across various boattail angles, and numerical simulations conducted on models featuring these optimal grooves further validate the ANN's accuracy in predicting drag coefficients, with a negligible deviation of only 0.98%. Additionally, analysis of flow characteristics and aerodynamics aids in understanding factors contributing to drag reduction.

Keywords: Artificial Neural Network, drag coefficient, boattail, numerical simulation.

1. Introduction

In daily life, blunt-base bodies are ubiquitous, such as trains, airplanes, UAVs, or road tankers. As a result, these bodies exhibit a significant separation region at the afterbody, contributing to substantial aerodynamic drag. Consequently, numerous studies have been conducted to enhance the aerodynamic performance of such models. Among these, utilizing a boattail proves to be a simple yet highly effective method [1-4]. The boattail serves to reduce and decelerate flow separation, thus mitigating drag force. However, flow around these bodies remains complex during motion, with flow separation phenomena persisting even at small boattail angles, leading to substantial drag induced by the boattail shape. Several methods have been proposed to further reduce drag on boattail bodies, including the use of grooves, which have demonstrated effectiveness in previous studies [5, 6]. However, these grooves are characterized by various geometric parameters, and the relationship between drag force and these parameters is highly intricate, not accurately representable by simple physical equations. Moreover, existing studies have primarily focused on specific boattail angles, failing to elucidate the influence of

longitudinal and transverse groove parameters on flow characteristics and other aerodynamic properties, and lacking recommendations for groove selection. Therefore, comprehensive research on the overall impact of grooves and the identification of optimal parameter sets for grooves to reduce drag are imperative to advance our understanding and improve aerodynamic performance.

There are many methods to determine the drag coefficient and aerodynamic characteristics of an object, such as experimental methods, CFD numerical simulation, discrete vortex method, etc. However, while experimental and numerical simulation methods yield highly accurate results, they require significant computational time and cost. Conversely, simpler methods with fast computational times like the discrete vortex method have lower accuracy. In practice, there are problems that require us to compute and recompute aerodynamic coefficients many times, especially in optimization problems. Therefore, experimental or numerical simulation methods are not efficient to use.

In recent years, the remarkable advancement of Artificial Neural Networks (ANNs) has revolutionized various aspects of the aerospace industry. Particularly noteworthy is their application in predicting the aerodynamic coefficients of flying objects, a field garnering significant attention. ANNs, equipped with the capability to learn from vast and intricate datasets, have emerged as indispensable tools for this purpose. Leveraging data encompassing the geometric and physical attributes of flying objects, alongside insights from simulations and flight tests, ANN networks adeptly learn and forecast aerodynamic coefficient values with remarkable precision. The integration of ANNs in aerodynamic coefficient prediction not only streamlines the aircraft design process, reducing time and costs, but also yields profound insights into the determinants of flight performance. This empowers designers and engineers to refine aircraft designs, optimizing performance metrics such as fuel efficiency, while upholding stringent standards of safety and reliability during operation.

Several studies have employed Artificial Neural Networks (ANNs) to predict aerodynamic coefficients. In a study by Nguyen et al. [7], a 3-layer ANN network trained with the Levenberg-Marquardt method was utilized to investigate the energy-optimal wing kinematics of a hovering bionic hawkmoth model. The authors utilized the ANN network to forecast aerodynamic forces generated during the hovering process, providing valuable data for optimization problems solved using genetic algorithms. Jaffar [8] employed various deep learning models, including 4-layer and 5-layer ANN models, to predict the drag coefficient of vehicle convoys on roads. Training and testing data were generated using Computational Fluid Dynamics (CFD) methods, revealing that the 4-layer ANN model accurately predicted this aerodynamic parameter with minimal computational time. Thirumalainambi [9] investigated the influence of activation functions and input data quantity on the predictive capabilities of ANN networks for aerodynamic coefficients. The findings suggested that ANN networks, when supplied with sufficient data, could effectively predict complex aerodynamic coefficients such as C_D, C_L and C_M. Furthermore, the sigmoid function employed in the hidden layer was identified as the most suitable for the 3-layer ANN network in predicting these aerodynamic coefficients.

In addition, there are many other studies that utilize ANN networks and various machine learning models to predict aerodynamic characteristics [10-13]. However, these studies often lack in-depth exploration of neural network design and specific investigation into the impacts of hyperparameters on network performance in predicting aerodynamic coefficients. Effective design of the ANN network is crucial for achieving accurate results, as various parameters can significantly influence the outcome of the problem. To comprehensively understand the behavior of ANN networks, this study will focus on investigating the influence of select hyperparameters, including the number of neurons in the hidden layer and the choice of activation function. By constructing an optimized ANN network, we aim to predict the drag coefficient of the model while systematically varying these parameters to identify the optimal set for accurate predictions.

2. Research model and Methodology

The aim of this study is to employ an Artificial Neural Network to optimize groove parameters that achieve maximum drag reduction for axisymmetric boattail models. The approach involves several steps, illustrated in Figure 1. Firstly, a dataset comprising 240 samples will be constructed using Computational Fluid Dynamics (CFD) simulations. This dataset will be divided into two subsets: 192 samples for training and validation, and 48 samples for independent testing. Throughout the network design process, various hyperparameters, including the number of neurons and activation functions, will be adjusted, and the ANN's performance will be assessed iteratively. The objective is to identify the most effective ANN configuration. Once the optimal design is determined, the ANN will be used to predict drag coefficients for axisymmetric boattail bodies. These predictions will inform the selection of the optimal groove parameters across different boattail angles (β).

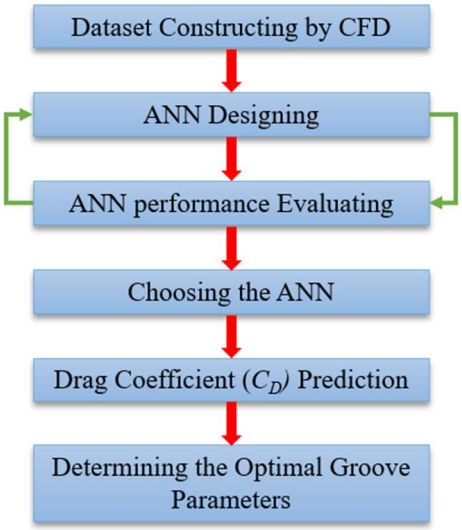

Figure 1 – Process flow diagram of ANN implementation

2.1 Research model

Figure 2 depicts the axisymmetric boattail bodies used in this study. Grooves are created along the trailing edge of the model. The model has a diameter D = 30 mm and a total length L = 251 mm. The nose of the model is elliptical to avoid flow separation on the surface. The boattail is conical with an angle β. The length of the boattail (L_b) is fixed at 0.7D. The model utilizes longitudinal grooves with parameters: groove diameter d; distance from the groove peak to the trailing edge (A); groove passing through the intersection of the boattail and the base.

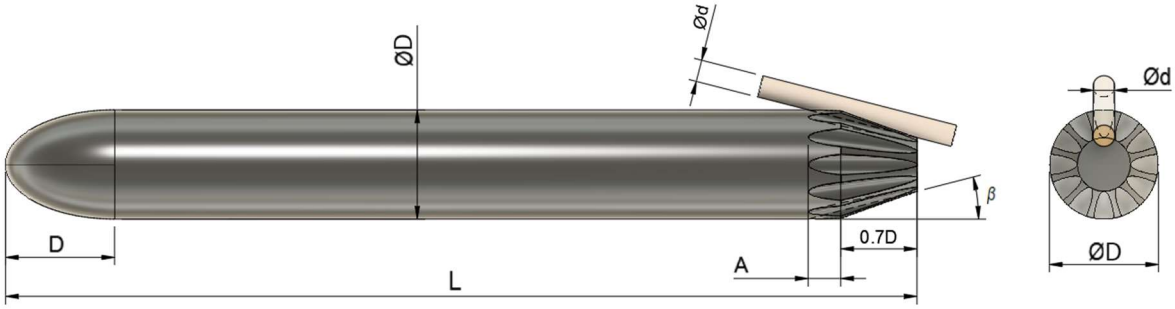

Figure 2 – Axisymmetric boattail models and definition of the groove cavities

The boattail angle β and groove parameters are systematically adjusted within the predefined limits outlined in Table 1. These specified ranges ensure the geometric integrity of the grooves, preventing issues such as groove intersections or the formation of holes in the model.

Table 1 – Groove parameters limits

Boattail Angle (β)	5-22°
Groove diameter (d)	3 ÷ 9 mm
Groove-peak Distance (A)	3 ÷ 9 mm
Number of grooves (n)	6-12

2.2 Computational method

To generate the dataset used for training and testing the ANN network, we utilized a numerical simulation method, specifically the Reynolds-Averaged Navier-Stokes (RANS) method with a turbulence model (k-ω SST). Figure 3 illustrates the computational domain used in this study.

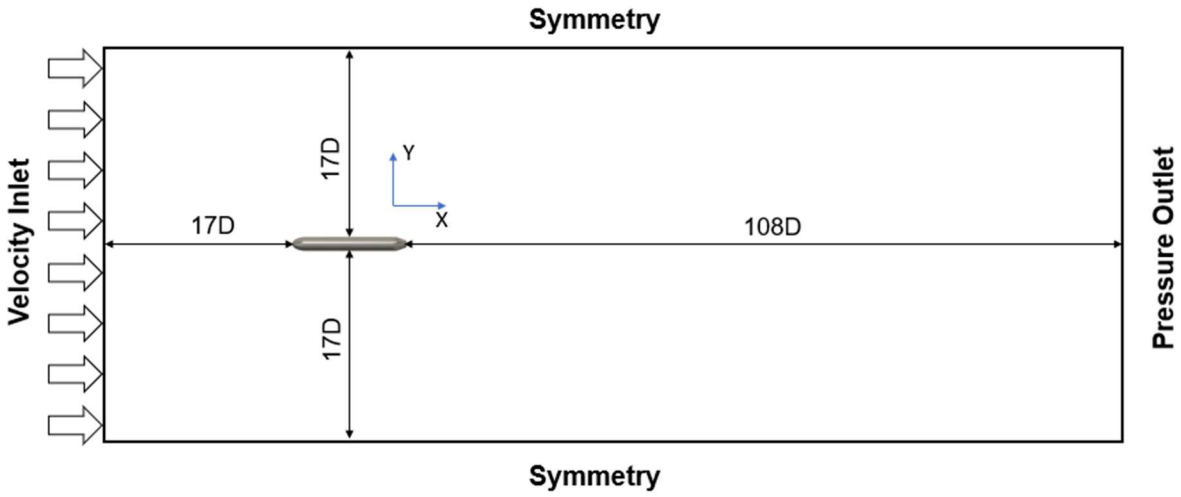

Figure 3 – Computational domain and boundaries

The computational domain has dimensions of 125D × 34D × 34D corresponding to length, width, and height. An inlet velocity of U_∞ = 22 m/s is applied to the upstream plane, at a distance of 17D ahead of the model nose. This velocity choice matches previous experiments in studies [2, 14] for the purpose of comparison and validating the accuracy of the results. The Reynolds number based on the diameter of the model is Re = 4.34×10^4. The boundaries of the computational domain use Symmetry conditions. In this study, we utilized the licensed commercial software ANSYS Fluent for simulation. The Coupled algorithm was selected with convergence criteria set to a residual tolerance of 10^{-6}.

The computational volume is discretized using an unstructured mesh, with the surface mesh of the research model depicted in Figure 4. To adhere to the requirements of the k-ω SST turbulence model, the first cell height from the model surface is set to 8.5×10^{-5} m, with a growth ratio of 1.18 for subsequent layers. This configuration ensures that the resulting value of y+ on the model surface, illustrated in Figure 4d, remains below 5.5. The total number of grid cells utilized for the simulation amounts to 3.7 million.

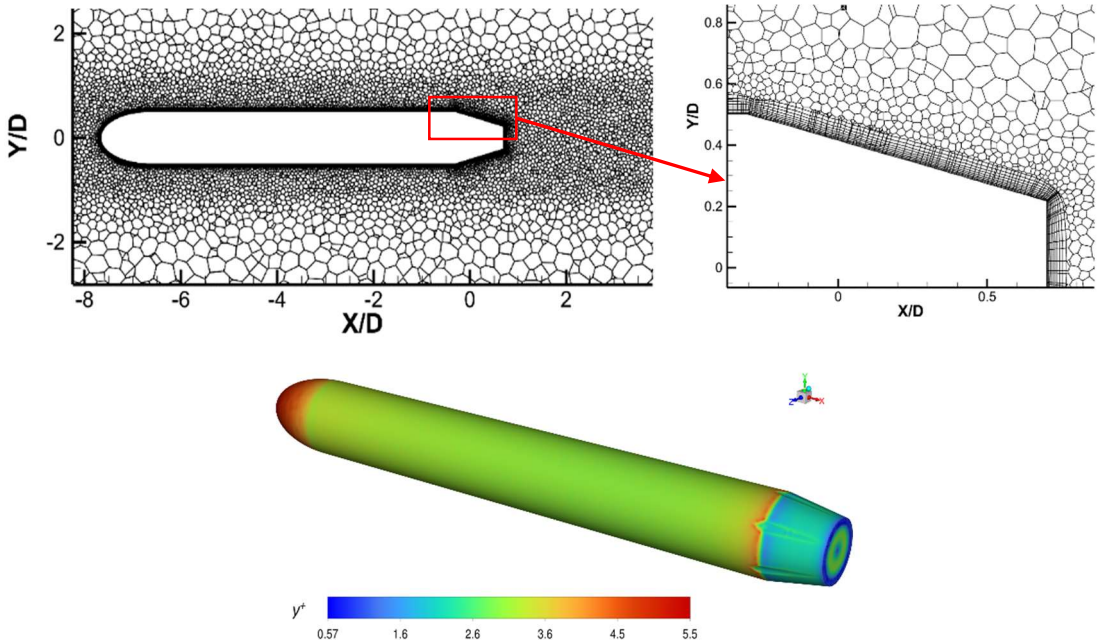

Figure 4 – Unstructured mesh and y^+ around the model

The numerical simulation results undergo validation through comparison with the findings of Tran et al. [1], as depicted in Figure 5. Notably, close alignment is evident between the outcomes of the two computational models, exhibiting an average discrepancy of ≤ 2.3%. These findings affirm the appropriateness and high accuracy of the computational model employed in this study, thus establishing its suitability for training the ANN network.

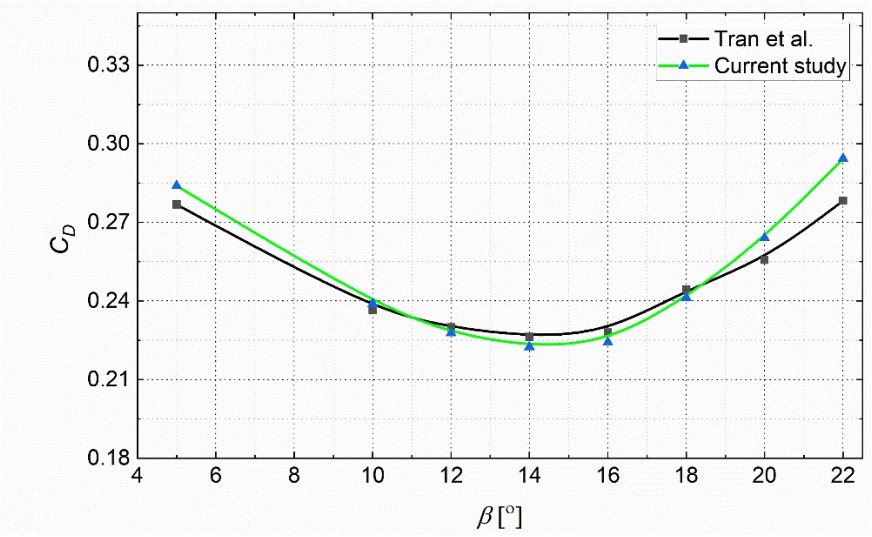

Figure 5. Comparison of the drag coefficient results of the model between numerical simulation and Tran's study [10].

2.3 Artificial Neural Networking

Artificial neural networks fundamentally comprise interconnected nodes, mimicking the functionality of neurons. They are employed to tackle intricate problems by leveraging learning acquired during the training phase, rather than solely relying on the analysis of physical properties [7]. In this study, we aim

to construct an artificial neural network tasked with predicting the drag coefficient, utilizing predefined geometric parameters as input variables.

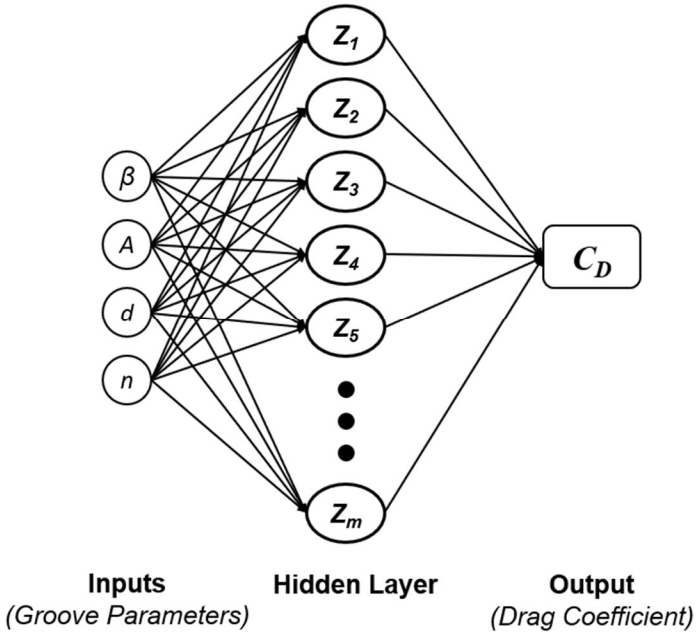

Figure 6 – Diagram of the Artificial Neural Network

The artificial neural network architecture is illustrated in Figure 6, comprising three layers: The input layer, which includes parameters such as the trailing edge angle (*β*), groove-peak distance (*A*), groove diameter (*d*), and the number of grooves (*n*). These parameters delineate the geometric characteristics of the longitudinal grooves. The hidden layer, denoted by neurons *Z*, is employed in this study as a single hidden layer, which has been shown in prior research [3, 4, 5] to be effective in predicting aerodynamic coefficients. The hidden layer accommodates a variable number of neurons, determined by the specific problem. In this study, we explore values ranging from 5 to 100 neurons to identify the optimal configuration. The output layer, which encompasses the drag coefficient as the sole parameter in this particular problem.

The neural network utilizes continuous transformations from input data passing through hidden layers via linear transformations, represented by the formula below:

$$z = w_1 x_1 + w_2 x_2 + w_3 x_3 + ... + w_n x_n + b = \sum_{i=1}^{n} w_i x_i + b \tag{1}$$

Here, w_i represents the weights of the input variables, x_i denotes the input variables, *n* is the number of input variables, and *b* is the bias adjustment coefficient. The bias adjustment coefficient functions akin to additional neurons that are not directly connected to preceding layers. By utilizing bias adjustment coefficients, we can dynamically shift the activation function position at neurons to the right or left, enhancing the flexibility of the network's training process and potentially boosting its efficiency [7].

After traversing the hidden layer, the neural network proceeds to employ nonlinear transformations facilitated by activation functions. These functions play a pivotal role in both the training and operation

of artificial neural networks, defining their nonlinear characteristics and learning capabilities. Various activation functions exist, with the following being commonly employed for predicting aerodynamic coefficients [15]:

- Sigmoid Function (*Logsig*):

$$\sigma(z) = \frac{1}{1+e^{-z}} \tag{2}$$

- Hyperbolic Tangent Sigmoid Function (*tanh*):

$$\sigma(z) = \frac{e^{z} - e^{-z}}{e^{z} + e^{-z}} \tag{3}$$

Loss Function optimization involves adjusting the parameters of the ANN to minimize its value. This optimization task is commonly accomplished using specialized algorithms. Various algorithms can be utilized for this purpose, including Levenberg-Marquardt (LM), Bayesian Regularization (BR), Gradient Descent with Momentum (GD), among others. In this study, we opt for the LM algorithm, as previous research has demonstrated its efficacy in predicting aerodynamic coefficients [7, 10, 12].

Before the artificial neural network can make predictions, it must undergo a training process. This involves iterative adjustments to the network's weights, biases, and hyperparameters, enabling it to effectively learn and represent input data while producing accurate output results. For training, we utilize predefined data known as training data, which in this study comprises 192 sets of groove parameters along with corresponding drag coefficient values computed by CFD. Of this data, 80% is allocated for training purposes, while the remaining 20% is reserved for validation. Additionally, a separate dataset consisting of 48 samples is designated for independent testing of the trained ANN. To assess the neural network's performance, we employ metrics such as Mean Squared Error (MSE), Coefficient of Determination (R), and Margin of Deviation (MoD) [xx], as defined by the formulas below:

$$MSE = \frac{1}{m}\sum_{i=1}^{m}(y_i - y_{ANNi})^2 \tag{4}$$

$$R^2 = 1 - \frac{\frac{1}{m}\sum_{i=1}^{m}\left(y_i - y_{ANNi}\right)^2}{\frac{1}{m}\sum_{i=1}^{m}\left(y_i - \overline{y}\right)^2} \tag{5}$$

$$MoD(\%) = \left[\frac{y_i - y_{ANNi}}{y_i}\right] \times 100 \tag{6}$$

Where: m the number of test samples, y_i the actual value of the i-th data sample and y_{ANNi} is the predicted value by the ANN for the i-th data sample.

3. Results

3.1. Optimal artificial neural network

The number of neurons in the hidden layer of the ANN serves as a crucial hyperparameter, exerting a substantial impact on the network's performance and generalization capabilities. It essentially mirrors the model's complexity. A large number of neurons can create a more complex model capable of learning more complex relationships in the data. Nevertheless, an excessive number of neurons may trigger overfitting. Conversely, too few neurons may result in underfitting, characterized by the model's inability to grasp the intricate patterns within the data.

Additionally, the choice of activation function is a crucial part of designing and training neural networks and can impact the network's performance. In reality, many problems cannot be solved using linear functions alone. For ANN, several nonlinear activation functions are used, such as *Sigmoid*, *Tanh*, or *ReLU* for hidden layers. For regression problems, the output layer typically uses the linear activation function, Pureline. Experimenting with and adjusting different activation functions is an important part of the model development process. In this study, we will sequentially use two activation functions: *sigmoid* and *tanh*. For each activation function, the number of neurons will vary from 5 to 100. The performance of the ANN will then be demonstrated in Tables 2 and 3.

Table 2 – Influence of the number of neurons on ANN performance with Tanh activation function

Order	No. of Neurons	Training		Validation		Testing	
		MSE	R	MSE	R	MSE	MoD
1	5	9.2808e-06	0.99229	1.3460e-05	0.98782	1.7133e-05	1.092
2	6	5.6915e-06	0.99507	1.9956e-05	0.98385	1.1636e-05	0.954
3	7	1.1027e-05	0.99095	1.0295e-05	0.99045	1.4295e-05	1.155
4	8	5.6152e-06	0.99505	5.9724e-06	0.99547	1.5533e-05	1.166
5	9	1.1378e-05	0.98735	4.4361e-06	0.98200	3.1602e-05	1.180
6	**10**	**1.7955e-05**	**0.98605**	**1.1258e-05**	**0.99211**	**1.6512e-05**	**0.973**
7	11	1.8326e-05	0.98391	1.4138e-05	0.99058	1.5228e-05	1.200
8	12	2.1615e-06	0.99813	6.7632e-06	0.99470	1.7727e-05	1.098
9	13	8.1653e-06	0.99310	1.0981e-05	0.99368	1.5533e-05	1.229
10	14	6.0715e-06	0.99443	1.2907e-05	0.99167	1.4557e-05	1.177
11	15	7.3821e-06	0.99369	5.2352e-06	0.99613	1.2759e-05	0.962
12	16	3.4808e-06	0.99691	1.5090e-05	0.98921	2.2613e-05	1.426
13	17	8.0513e-06	0.99351	1.1927e-05	0.98691	2.0375e-05	1.299
14	18	4.0279e-06	0.9965	8.7860e-06	0.99288	1.6950e-05	1.019
15	19	1.5970e-06	0.99871	1.1736e-05	0.98696	2.4079e-05	1.330
16	20	1.5993e-05	0.98749	2.0274e-05	0.9902	1.6542e-05	1.300
17	30	2.8670e-07	0.99976	6.8802e-05	0.93926	2.9105e-05	1.752
18	40	1.9168e-06	0.99852	3.5979e-05	0.96925	4.5016e-05	2.050
19	50	7.0026e-08	0.99994	6.0782e-05	0.93971	4.0529e-05	1.837
20	100	1.3289e-07	0.9999	2.9098e-04	0.72237	2.8107e-04	5.742

Table 3 – Influence of the number of neurons on ANN performance with Sigmoid activation function

TT	No. of Neurons	Training		Validation		Testing	
		MSE	R	MSE	R	MSE	MoD
1							
	5	5.4627e-06	0.99506	6.3034e-06	0.99546	1.0908e-05	0.769
2	6	4.5144e-06	0.9961	4.8708e-05	0.96049	1.1367e-05	1.042
3	7	1.9375e-05	0.98365	1.6771e-05	0.98465	1.1896e-05	1.031

4	8	7.4802e-06	0.99357	1.6150e-05	0.98653	1.9390e-05	1.087
5	9	3.1841e-06	0.99762	7.1926e-06	0.99511	9.8332e-06	0.830
6	**10**	**1.9369e-06**	**0.9983**	**3.3445e-06**	**0.99755**	**1.1155e-05**	**0.760**
7	11	3.2232e-06	0.9971	6.8419e-06	0.99535	1.1484e-05	0.938
8	12	2.6002e-06	0.99788	6.5503e-06	0.99468	9.7357e-06	0.877
9	13	4.6928e-06	0.99644	1.0625e-05	0.98491	1.3049e-05	0.895
10	14	9.0857e-06	0.99282	1.4778e-05	0.98477	1.6831e-05	1.053
11	15	3.3892e-06	0.99711	1.6504e-05	0.98666	1.6913e-05	1.216
12	16	1.3023e-06	0.99887	2.9732e-05	0.9765	1.3746e-05	0.944
13	17	2.5585e-06	0.99791	1.0414e-05	0.98974	1.6276e-05	1.216
14	18	1.0879e-05	0.99105	2.3677e-05	0.97683	2.0296e-05	1.424
15	19	5.7890e-07	0.99921	2.4832e-05	0.99202	1.9540e-05	1.280
16	20	5.1955e-06	0.99528	2.0221e-05	0.98579	2.4963e-05	1.423
17	30	6.4186e-07	0.99945	1.4319e-05	0.9892	3.1739e-05	1.704
18	40	9.8363e-07	0.99915	1.9072e-05	0.98628	3.0750e-05	1.621
19	50	3.6777e-07	0.98649	3.6191e-05	0.9468	4.4685e-05	1.989
20	100	9.1092e-07	0.99923	9.0503e-05	0.93304	1.3383e-04	3.466

Analysis of the two tables reveals a striking similarity in the effectiveness of neural networks employing sigmoid and tanh activation functions. Optimal performance is observed within the 5-20 neuron range for both functions. However, beyond 20 neurons, while the networks exhibit excellent performance during training, their validation and testing results deteriorate, indicative of overfitting. Closer scrutiny of the data unveils a marginally superior performance of the network utilizing the sigmoid function compared to tanh. Notably, peak performance for both networks is attained with 10 neurons in the hidden layer, denoted in red. Thus, the combination of sigmoid function and 10 neurons emerges as the most favourable hyperparameters for predicting drag coefficients of axisymmetric boattail models.

After finalizing the selection of features and hyperparameters, the neural network undergoes training and validation using the available dataset, as outlined previously. Figure 7 showcases key outcomes of this training process. Notably, at epoch 16, training halts as the validation MSE achieves its optimal value of 3.3445e-06, while the training MSE stands at 1.9369e-06 (refer to Figure 7a). This intervention is crucial to forestall overfitting, wherein validation MSE escalates while training MSE continues to decline. At this point, errors generated by the ANN for both training and validation datasets are minimal, largely concentrated within the range of -0.00213 to 0.002545 (depicted in Figure 7b). Furthermore, in Figure 7c, we observe that the Coefficient of Determination values for both the training and validation processes are approaching 1, with values of 0.9983 and 0.9976, respectively. These near-perfect scores attest to the high efficacy and accuracy of the trained ANN outputs.

After training, the ANN is independently tested with 48 samples. The results of the testing process are shown in Figure 8. It can be observed that the predicted values by the ANN closely match the accurate values (determined by the CFD method). The majority of errors are below 1%, with the largest error recorded at 4.7%, and an average error of only 0.76%. This once again confirms the accuracy of the outputs generated by the ANN. Consequently, it ensures the reliability of using the ANN results for determining the optimal parameters of the longitudinal grooves to reduce drag for axisymmetric boattail models.

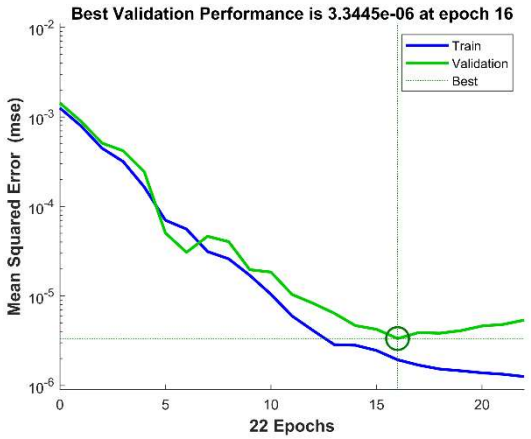

(a) Mean Square Error (MSE)

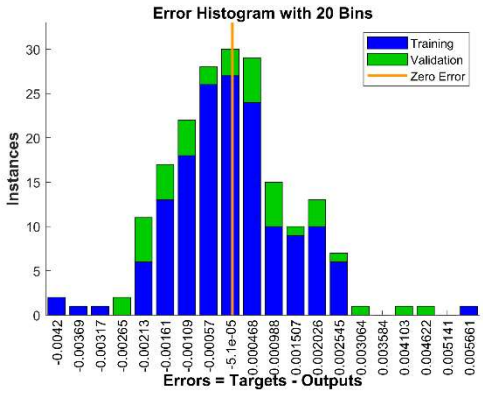

(b) Error

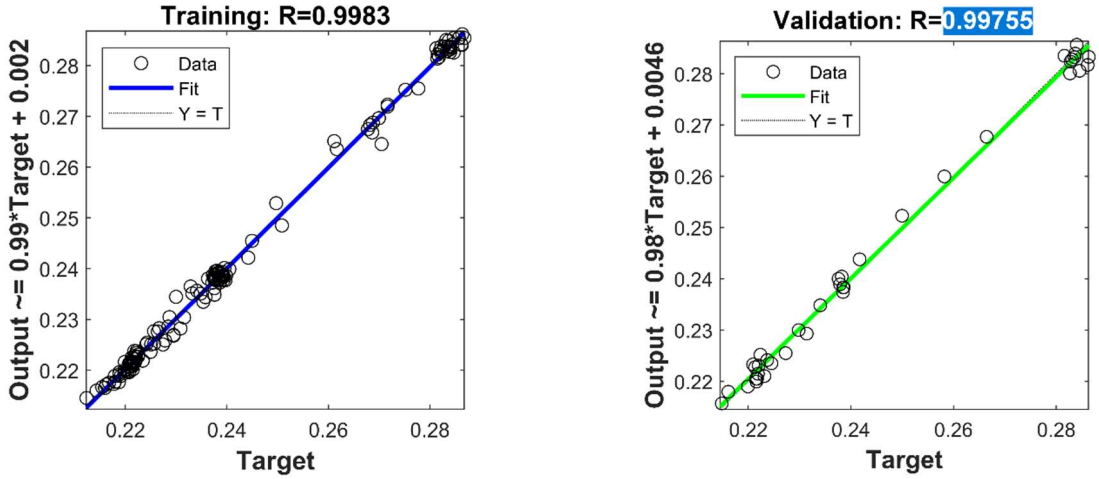

(c) Coefficient of Determination (R)

Figure 7 – Performance of ANN

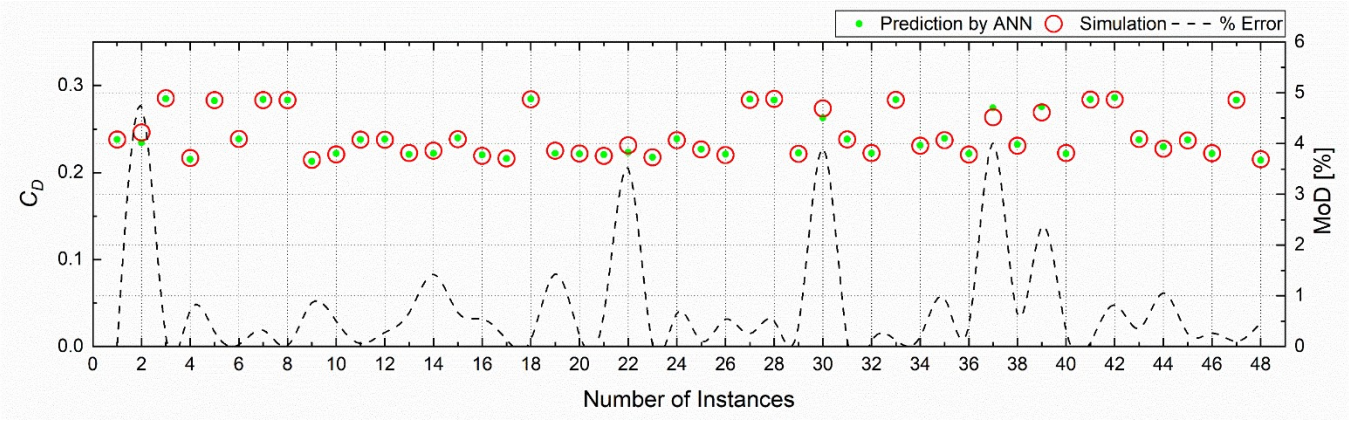

Figure 8 – Comparison of results generated by ANN and CFD

3.2 Optimal groove parameters

After the training and testing process, the ANN was employed to predict the drag coefficient for axisymmetric boattail models with varying groove parameters as specified in Table 1. Here, β ranges

from 5-22º with a step of 1º; *A* and *d* vary from 3-9 mm with a step of 1 mm; *n* changes from 6-12 grooves with a step of 2 grooves to ensure axial symmetry. Therefore, we have a total of 3528 cases for the ANN to predict. Among these outputs, for each *β* angle, we selected a set of groove parameters where the CD coefficient produced was minimized. Consequently, we compiled Table 4 consisting of the optimal groove parameters for each β angle.

After completing the training and testing phases, the ANN was utilized to forecast the drag coefficient for axisymmetric boattail models, considering varied groove parameters outlined in Table 1. Specifically, *β* ranges from 5-22º with a step of 1º; *A* and *d* vary from 3-9 mm with a step of 1 mm; *n* ranges from 6-12 grooves with a step of 2 grooves to ensure axial symmetry. Thus, a total of 3528 cases were generated for the ANN to predict. From these outputs, a set of groove parameters minimizing the C_D coefficient was selected for each *β* angle. Consequently, Table 4 was compiled, presenting the optimal groove parameters corresponding to each *β* angle.

Looking at this set of optimal parameters, we observe that at $\beta = 5^o$, the drag coefficient is minimized when the groove parameters are at their smallest values. The groove parameters then gradually increase as *β* increases, reaching their maximum values when $\beta > 19^o$. The minimum value of C_D is achieved at the 16th parameter set, corresponding to $\beta = 20^o$, $A = 9$ mm, $d = 9$ mm, and $n = 12$ grooves. However, the difference between it and the C_D values at neighboring parameter sets is not significantly large.

Table 4 – Optimal groove parameters according to the *β* angle

Order	***β***	***A***	***d***	***n***	C_D
1	10	3	4	8	0.2356
2	11	3	5	8	0.2290
3	12	4	8	12	0.2241
4	13	5	8	12	0.2207
5	14	5	8	12	0.2187
6	15	6	8	12	0.2174
7	16	8	8	12	0.2165

3.3 Analysis the effect of optimal grooves on aerodynamic characteristics of boattail models

To confirm the accuracy of the optimized values predicted by the ANN, in this section, numerical simulations are conducted. Figure 9 presents a comparison chart of the computed values using the CFD method and predicted by the ANN for the model containing the optimized grooves. Additionally, the drag coefficient values for the case without grooves are included to illustrate the difference between the ungrooved case and the optimized groove case. It is observed that the values predicted by the ANN and computed by CFD are very close, with the largest deviation being 1.87% and the average deviation being 0.98%. Furthermore, comparing with the ungrooved case, we find that the drag coefficient remains relatively unchanged for $\beta \leq 14^o$; however, it decreases significantly when $\beta > 14^o$, dropping by over 27% at a boattail angle of 22º.

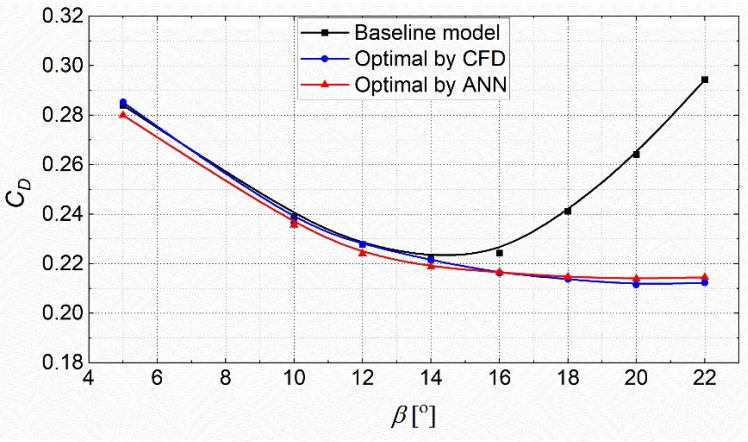

Figure 9 – The drag coefficient for the optimized groove parameter sets

We continue analyzing the flow characteristics and aerodynamics for the model equipped with the optimized grooves at a 20º boattail angle, thereby understanding the reasons behind the significant reduction in drag. Figure 10 illustrates the streamlines on the boattail surface for two cases: without the grooves and with the optimized grooves. It is evident that with the optimized grooves, the flow on the boattail surface becomes smooth and attached, which contrasts sharply with the fully separated flow observed when there is no groove. This observation aligns with the findings of the study [5] by Howard et al. Additionally, we can also observe that the length of the recirculation zone behind the tail significantly decreases with the optimized grooves compared to when there is no groove.

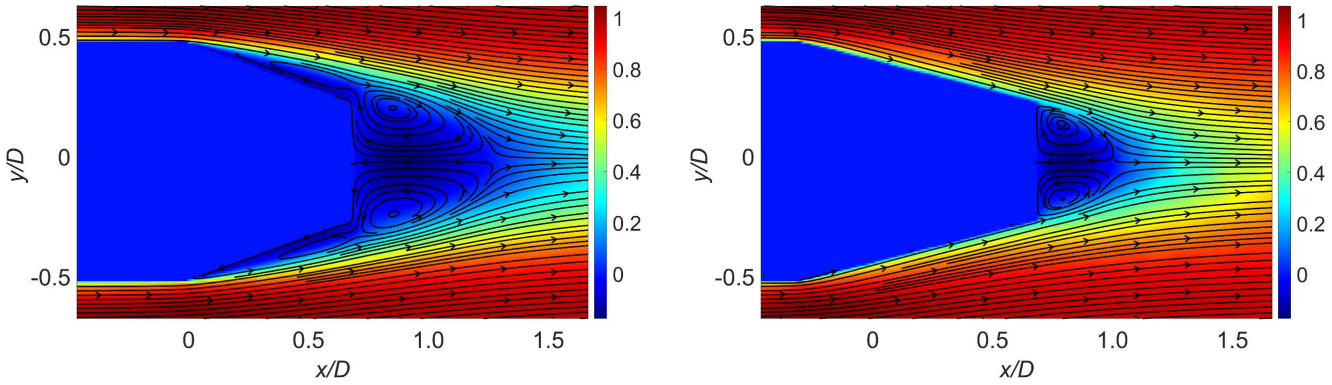

Figure 10 – Streamlines around the boattails without the grooves (left) and with the optimized grooves (right)

The phenomenon of flow separation or attached flow can also be inferred through the analysis of the distribution of the skin friction coefficient on the boattail surface, as indicated in Figure 11. In the case without the groove, corresponding to the baseline model, we observe that the skin friction coefficient C_{fx} mostly has negative values, indicating that the flow is completely separated. Conversely, when the optimized groove is present, the C_{fx} values are positive over the entire boattail, indicating that the flow is totally attached.

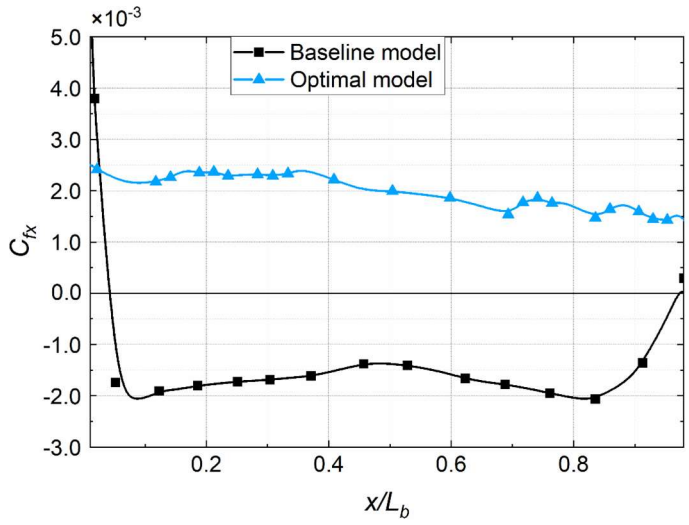

Figure 11 – Skin-friction coefficient distribution on boattail surface

The pressure distribution on the surface plays an important role in comprehending the mechanisms behind drag reduction. Figure 12 depicts the pressure coefficient distribution on the boattail surface with optimized grooves and without grooves. We observe that the pressure coefficient forms a bottom at the boattail shoulder location and gradually increases along the surface. With the optimized grooves, induced geometric changes shift this C_p bottom forward by a distance equal to A. Furthermore, the minimum C_p value with the optimized grooves is lower than that in baseline case, potentially due to localized flow separation at the groove shoulder. Beyond this region, the pressure coefficient rises rapidly, surpassing the baseline case. This alteration contributes significantly to the decrease in the model's drag.

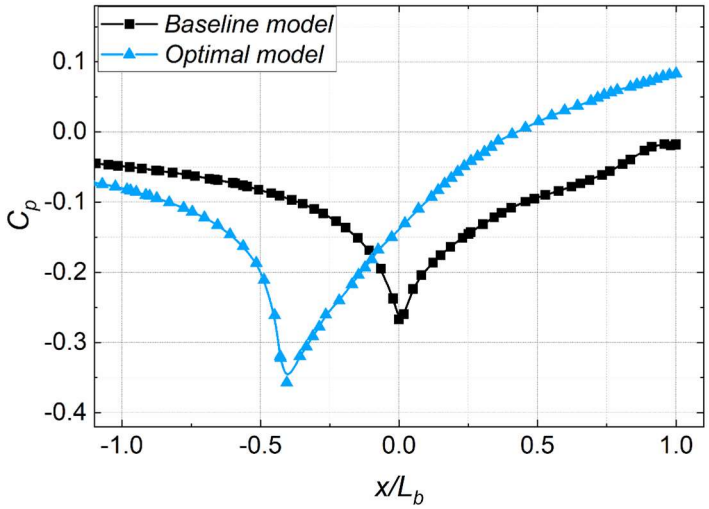

Figure 12 – Pressure Coefficient distribution on boattail surface

4. Conclusion

The paper has presented the process of designing an artificial neural network to predict the drag coefficient for axisymmetric boattail models with longitudinal grooves on the boattail surface. The hyperparameters of the neural network were specifically investigated to find the most suitable design for the problem. After training, the neural network was tested with independent data. The results showed

that the error between the accurate values and the predicted values of the network was less than 4.7% on average about 0.76%. This confirms the reliability of the artificial neural network used in this study. Using the obtained ANN to predict the drag coefficient of the axisymmetric boattail models helped determine the optimal parameters for the longitudinal grooves in reducing drag. The predicted drag coefficient when using the optimized grooves, as simulated numerically, once again confirmed the accuracy of the ANN predictions, with an average error of only 0.98% and a maximum error not exceeding 2%. Notably, the minimum drag coefficient was attained at a boattail angle (β) of 20º, with groove parameters (*A, d, n*) of 9 mm, 9 mm, and 12 grooves, respectively. Comparison with ungrooved models revealed a significant reduction in drag for $\beta > 14º$, decrease by over 27% at a boattail angle of 22º. Analysis of flow and aerodynamic features also revealed that the main reason for the reduction in drag was due to the use of grooves, which made the flow smoother, eliminated separation, and increased pressure on the tail surface.

5. Contact Author Email Address

The contact author email address: raketavn@gmail.com

6. Copyright Statement

Acknowledgments

This research is funded by Vietnam National Foundation for Science and Technology Development (NAFOSTED) under grant number 107.03-2021.52.

References

[1] Tran T.H. Journal of Mechanical Science and Technology. *Effect of boattail angle on near-wake flow and drag of axisymmetric models: a numerical approach,* Vol. 35, pp 563-573, 2021.

[2] Tran T.H. Experimental Thermal and Fluid Science. *Effect of boattail angles on the flow pattern on an axisymmetric afterbody surface at low speed*, Vol. 99, pp 324-335, 2018.

[3] Tran T.H. International Journal of Aerospace Engineering. *The effect of boattail angles on the near-wake structure of axisymmetric afterbody models at low-speed condition*, Vol.62, No.4, pp. 1-14, 2020.

[4] Mair W. Aeronautical Quarterly. *Reduction of base drag by boat-tailed afterbodies in low-speed flow*, Vol. 20, No. 4, pp 307-320, 1969.

[5] Howard F.G, W.L. Goodman. Journal of aircraft. *Axisymmetric bluff-body drag reduction through geometrical modification*, Vol. 22, No. 6, pp 516-522, 1985.

[6] A. Mariotti, A., G. Buresti, G. Gaggini, and M. Salvetti. Journal of Fluid Mechanics. *Separation control and drag reduction for boat-tailed axisymmetric bodies through contoured transverse grooves,* Vol. 832, pp 514-549, 2017.

[7] Nguyen A.T. Journal of Bionic Engineering. *A neural-network-based approach to study the energy-optimal hovering wing kinematics of a bionic hawkmoth model*, Vol. 16, pp 904-915, 2019.

[8] Jaffar F. IEEE Access. *Prediction of drag force on vehicles in a platoon configuration using machine learning,* Vol. 8: p. 201823-201834, 2020.

[9] Thirumalainambi R, and J. Bardina. Proceedings of SPIE. *Training data requirement for a neural network to predict aerodynamic coefficients*. in *Independent component analyses, wavelets, and neural networks*, Vol. 5102, 2003.

[10] Kurtulus D.F. Neural Computing and Applications. *Ability to forecast unsteady aerodynamic forces of flapping airfoils by artificial neural network*, Vol. 18, pp 359-368, 2009.

[11] Rehman K.U., A.B. Çolak, and W. Shatanawi. Mathematics. *Artificial neural networking (ANN) model for drag coefficient optimization for various obstacles*, Vol. 10, No. 14, pp 2450, 2022.

[12] Rajkumar T., C. Aragon, J. Bardina, and R. Britten. WIT transactions on information and communication technologies. *Prediction of aerodynamic coefficients for wind tunnel data using a genetic algorithm optimised neural network*, Vol. 28, 2002.

[13] Rajkumar T., and J.E. Bardina. FLAIRS Conference. *Prediction of Aerodynamic Coefficients Using Neural Networks for Sparse Data*. Florida, USA, Vol. 02, pp 242-246, 2002.

[14] Tran T.H. Experiments in Fluids. *Effect of Reynolds number on flow behavior and pressure drag of axisymmetric conical boattails at low speeds,* Vol. 60, pp 1-19, 2019.

[15] Feng J. and S. Lu. Journal of physics: conference series. *Performance analysis of various activation functions in artificial neural networks*, 2019.